A LINEARIZED NON-ISOTHERMAL GENERAL RATE MODEL FOR STUDYING THERMAL EFFECTS IN LIQUID CHROMATOGRAPHIC COLUMNS

by

Nadia KIRAN[a], Sadia PERVEEN[b*], Seemab BASHIR[b], and Shamsul QAMAR[a,c]

[a] Department of Mathematics, COMSATS University Islamabad, Islamabad, Pakistan
[b] Department of Mathematics, AIR University, Islamabad, Pakistan
[c] Max Planck Institute for Dynamics of Complex Technical Systems Magdeburg, Magdeburg, Germany

Original scientific paper
https://doi.org/10.2298/TSCI200729336K

A linearized non-isothermal general rate model is formulated and analytically solved to quantify the effects of temperature variations in fixed-bed chromatographic columns. The model contains a set of four coupled PDE accounting for energy transfer resistances, inner and outer particle-pore diffusions, and interfacial mass and axial dispersion. The Laplace transform, the eigenvalue-decomposition technique, and a conventional technique for the solutions of ODE are jointly employed for the solution of the model equations. A few numerical test studies are considered to assess the impact of system parameters on the performance of packed-bed adsorption columns. To access the range of applicability and to get the scope of the appropriateness of calculated analytical results, the numerical results are also obtained by applying a high resolution finite volume scheme. The analytical solutions obtained can be used as an invaluable tool for analyzing, optimizing, and upgrading the non-isothermal liquid chromatographic procedures.

Key words: *linearized isotherm, thermal effects, analytical solutions, non-isothermal chromatography, general rate model, numerical solutions, finite volume scheme*

Introduction

Chromatography is a proven method for separating complex chemical samples into its individual constituent. The high performance liquid chromatography (HPLC) has been extensively applied for the large-scale separations in pharmaceutical and chemical industries, [1-3]. This process has capability to separate multi-component mixtures and to ascertains their features like chemical structure and concentration. Since last few years, chromatographers have started using elevated temperature for the development and optimization of HPLC methods. High temperature liquid chromatography (HTLC) correlates to any separation which is performed at temperatures ranging between 40-200 °C using a liquid mobile phase, [4]. The HTLC has profound benefits as compared to the traditional ambient HPLC, because in the HTLC analysis, thermodynamics and kinetic parameters are functions of the temperature. The HTLC reduces retention time, increases column efficiency, provides greater compatibility for longer

* Corresponding author, e-mail: sadia.ahsan@mail.au.edu.pk

columns packed with smaller particles, minimizes (or excludes) the use of organic solvent involved in the bulk phase, enhances selectivity and resolution, and has the ability to perform a temperature programmed elution. Moreover, reproducibility can be improved through a controlled temperature.

Until recent times, temperature was not considered as a variable in a typical HPLC process. It is because of the fact that composition of the mobile phase, which has greater effect on selectivity, can easily be adapted for optimization of the process. Over the past two decades variations in the column temperature have been explored. Literature review for the past decade shows that interest in the use of HTLC has gained momentum principally as a way to increase the speed of LC analysis and to modify chromatographic selectivity, [5]. Several experimental studies have been conducted to study temperature variations inside the column and their consequent on the chromatographic process, [6-10]. Thermal effects in gas chromatography were also analyzed and reported by several authors, [11-15]. The effects of zone cooling to facilitate the flow of analyte for large injected volume within packed-capillaries were discussed by [9, 16]. Furthermore, Antia and Horvath [5] have examined the conditions for quick separation of large molecules at elevated temperatures in HPLC. Other contributions regarding temperature variations inside liquid chromatographic columns can be found in the articles [17-21]. Moreover, [22-27] have theoretically investigated the effects of temperature changes by using non-isothermal dispersive equilibrium model (DEM) and kinetic lumped model (KLM).

The modelling of chromatographic procedures is usually carried out with mass-balance based macroscopic or deterministic models. In literature, the countless macroscopic models are present that illustrate the chromatographic procedures with numerous details [1, 2]. The macroscopic models like the ideal model (IM), DEM, KLM, lump pore diffusion model, equivalence of macroscopic kinetic model, and general rate model (GRM) have numerical or analytical solutions that can be derived with ease, normally by using well-established and standard mathematical software and tools. This article extends our previous analysis, c.f. [24, 25, 27], by formulating and solving analytically the non-isothermal GRM of liquid chromatography, which is one of the most detailed kinetic model that accounts for many of the factors influencing the process of chromatography. In the transparticle-transport mechanisms of non-isothermal GRM, the considerable contributions include the solid diffusion in the adsorbed phase, pore diffusion in fluid-filled pores, the intera-particle-dispersion, and intera-particle-transport mechanism depending on mixing (axial dispersion) effects, and resistances of interfacial mass and heat transfer. Thus the model mathematically represents a system of convection-diffusion partial differential equation. To obtain the analytical solution of governing model equations, the Laplace transformation and the eigenvalue-decomposition technique are employed. Here, an accurate and efficient numerical Laplace inversion is applied to acquire back the solution in the time domain, see [25, 28]. To determine ranges in which our analytical solutions are useful and valid, a second order finite volume scheme is also implemented to approximate the model equations. Both numerical and analytical solutions are compared with each other. Several case studies are being conducted to further exhibit the joint occurrence of concentration and thermal profiles and to point-out crucial parameters which effect the temperature variations inside thermally insulated columns.

The non-isothermal GRM of column chromatography

To formulate a non-isothermal GRM, the following basic assumptions are made.

– the column is insulated thermally and is filled homogeneously with spherical particles of radius R_p,

– an incompressible mobile phase is considered,
– constant volumetric flow rate is assumed,
– physical properties of the system like viscosity, density, heat capacity, transport coefficients like axial heat-conductivity, and the axial dispersion are assumed independent of temperature,
– the axial and heat conductivity coefficient are not depending on the flow rate, and
– the mobile phase (solvent) has no interaction with the stationary phase.

For the mobile phase, the GRM has two sets of coupled mass balances, one set indicates the bulk phase flow that moves in the interstitial stationary phase carrying various components. The second set describes the dynamics of solute in the stagnant fluid of particle pores. The governing mass balance equation for a single solute in the bulk phase is given, [2]:

$$\epsilon_b \frac{\partial c_b}{\partial t} + (1-\epsilon_b)\frac{3}{R_p} k_{\text{eff}} \left(c_b - c_p \mid_{R=R_p} \right) + \epsilon_b u \frac{\partial c_b}{\partial z} = \epsilon_b D_b \frac{\partial^2 c_b}{\partial z^2} \tag{1}$$

where $c_b(z, t)$ is the concentration of solute in the bulk fluid, ϵ_b – the external porosity, R_p – the radius of spherical solid particle, k_{eff} – the effective external coefficient of mass-transfer, the factor $3/R_p$ represents the ratio of surface area to volume for the spherical particles, $c_p(z, t, r)$ – the concentration of solute in the particle pores, the term $c_b - c_p|_{R=Rp}$ on the right reflects differences in concentration between the extra particular mobile phase through the external film, and the intra particular mobile phase at the particle surface. The u is the interstitial velocity, D_b – the coefficient of axial-dispersion, t – the time, and z – the column's axial-co-ordinate and the radial-co-ordinate of the spherical particle is denoted by R. The dynamics of solute concentration in the particle pores can be described by the mass balance equation:

$$\epsilon_p \frac{\partial c_p}{\partial t} + (1-\epsilon_p)\frac{\partial q_p}{\partial t} = D_{\text{eff}} \left[\frac{1}{R^2} \frac{\partial}{\partial R} \left(R^2 \frac{\partial c_p}{\partial R} \right) \right] \tag{2}$$

where ϵ_p is the internal particle porosity, $q_p(z, t, r)$ – the concentration of the solid-phase in equilibrium, and $D_{\text{eff}} = \epsilon_p D_p$ – the effective internal pore-diffusivity coefficient. The corresponding energy balance of the column is given:

$$\epsilon_b \frac{\partial T_b}{\partial t} + \epsilon_b u \frac{\partial T_b}{\partial z} = \frac{\lambda_{\text{eff},z}\epsilon_b}{\rho^L c_p^L} \frac{\partial^2 T_b}{\partial z^2} - \frac{3h_{\text{eff}}(1-\epsilon_b)}{R_p \rho^L c_p^L} \left(T_b - T_p \mid_{R=R_p} \right) \tag{3}$$

In the aforementioned energy balance equation, the symbol T_b denotes the bulk fluid temperature, T_p – the fluid temperature in the particle pores, $\lambda_{\text{eff},z}$ – the effective axial coefficient of heat conductivity, ρ^L indicates density per unit volume in the mobile phase, c_P^L symbolizes the mobil phase heat capacity, and h_{eff} defines the effective coeficient of heat transfer from particle to fluid. An energy balance law for the radial temperature profile inside the particles pores can be described:

$$\overline{\rho c_p} \frac{\partial T_p}{\partial t} + (1-\epsilon_p)(-\Delta H_A)\frac{\partial q_p}{\partial t} = \lambda_{\text{eff},e} \left[\frac{1}{R^2} \frac{\partial}{\partial R} \left(R^2 \frac{\partial T_p}{\partial R} \right) \right] \tag{4}$$

where $\overline{\rho c_p} = \epsilon_p \rho^L c_P^L + (1-\epsilon_p)\rho^S c_P^S$. Moreover, ΔH_A represents the enthalpy of adsorption, ρ^S – the density, c_P^S – the heat capacity in the solid phase, and $\lambda_{\text{eff},e}$ – the effective internal heat diffusivity coefficient. The considered densities ρ^L, ρ^S, and heat capacities c_P^L and c_P^S for the procedure are taken independent of temperature, which is a valid assumption in the case of limited temperature range. The amount of solute absorbed is dependent to the temperature that can be easily

revealed through van't Hoff-type expression considering the enthalpy of adsorption. Thus, the linear phase equilibrium relation in concentration is expresssed:

$$q_p(c_p,T_p)=a^{\text{ref}}c_p\exp\left[\frac{-\Delta H_{\text{A}}}{\text{R}_{\text{g}}}\left(\frac{1}{T_p}-\frac{1}{T^{\text{ref}}}\right)\right] \tag{5}$$

where a^{ref} measures the relative mass storage capacity of the solid phase at a reference temperature T^{ref} and the symbol R_{g} symbolizes the general gas constant. Let us define:

$$c_{b,1}=c_b,\ c_{b,2}=T_b-T^{\text{ref}},\ c_{p,1}=c_p,\ c_{p,2}=T_p-T^{\text{ref}} \tag{6}$$

Moreover, we introduce the following new variables in dimensionless form to reduce the number of involved parameters:

$$\begin{gathered}x=\frac{z}{L},\ \tau=\frac{ut}{L},\ r=\frac{R}{R_p},\ \text{Pe}_e=\frac{Lu}{D_b},\ \text{Pe}_T=\frac{Lu\rho^L c_P^L}{\lambda_{\text{eff},z}},\ \text{B}_c=\frac{k_{\text{eff}}R_p}{D_{\text{eff}}}\\ \text{B}_T=\frac{h_{\text{eff}}R_p}{\lambda_{\text{eff},e}},\ \eta_c=\frac{D_{\text{eff}}L}{R_p^2u},\ \eta_T=\frac{\lambda_{\text{eff},e}L}{R_p^2u\rho^L c_P^L},\ \xi_c=3\text{B}_c\eta_c F_b,\ \xi_T=3\text{B}_T\eta_T F_b\end{gathered} \tag{7}$$

where $F_b=(1-\epsilon_b)/\epsilon_b$ is the phase ratio, L – the axial length of column, Pe_e – the Peclet number for concentration, Pe_T – the Peclet numbers for temperature, B_c and B_T are the corresponding Biot numbers, respectively, while η_c, η_T, ξ_c, and ξ_T are the dimensionless constants. By utilizing eqs. (6) and (7) in eqs. (1)-(4), the system of equations becomes:

$$\frac{1}{\text{Pe}_m}\frac{\partial^2 c_{b,m}}{\partial x^2}-\frac{\partial c_{b,m}}{\partial x}=\frac{\partial c_{b,m}}{\partial \tau}+\xi_m\left(c_{b,m}-c_{p,m}\mid_{r=1}\right),\ \text{for}\ \ m=1,2 \tag{8}$$

$$\epsilon_p\frac{\partial c_{p,1}}{\partial \tau}+(1-\epsilon_p)\frac{\partial q_p}{\partial \tau}=\eta_c\left[\frac{1}{r^2}\frac{\partial}{\partial r}\left(r^2\frac{\partial c_{p,1}}{\partial r}\right)\right] \tag{9}$$

$$\left[\epsilon_p+(1-\epsilon_p)\frac{\rho^s c_P^s}{\rho^L c_P^L}\right]\frac{\partial c_{p,2}}{\partial \tau}+\frac{(1-\epsilon_p)\Delta H_A}{\rho^L c_P^L}\frac{\partial q_p}{\partial \tau}=\eta_T\left[\frac{1}{r^2}\frac{\partial}{\partial r}\left(r^2\frac{\partial c_{p,2}}{\partial r}\right)\right] \tag{10}$$

where eq. (8), we define $\text{Pe}_e=\text{Pe}_1$ and $\text{Pe}_T=\text{Pe}_2$, and similarly $\xi_c=\xi_1$ and $\xi_T=\xi_2$. The equilibrium relation between the solid and liquid-phase concentrations in eq. (5) can be linearized by using first order Taylor-expansion considering small variations in the temperature and concentration [24, 25]. The Taylors expansion is defined:

$$q_p(c_p,T_p)\approx q_p(c^{\text{ref}},T^{\text{ref}})+\frac{\partial q_p}{\partial T_p}_{(c^{\text{ref}},T^{\text{ref}})}(T_p-T^{\text{ref}})+\frac{\partial q_p}{\partial c_p}_{(c^{\text{ref}},T^{\text{ref}})}(c_p-c^{\text{ref}}) \tag{11}$$

Utilizing the Taylor's expansion up to first order in eq. (5), and simplifying the resulting expression, we get:

$$q_p(c_{p,1},c_{p,2})=a^{\text{ref}}c_{p,1}+a^{\text{ref}}c^{\text{ref}}\frac{\Delta H_{\text{A}}}{\text{R}_{\text{g}}(T^{\text{ref}})^2}c_{p,2} \tag{12}$$

The initial conditions for the previous model equations are defined:

$$c_{b,m}(x,0)=c_{b,m}^{\text{init}},\ c_{p,m}(x,0,r)=c_{p,m}^{\text{init}},\ \text{for}\ \ m=1,2\ \text{ and }\ 0\le x,r\le 1 \tag{13}$$

where $c_{b,1}^{\text{init}}$ is the initial liquid phase concentration, $c_{p,1}^{\text{init}}$ – the initial concentration in the particle pores, while $c_{b,2}^{\text{init}} = T_b^{\text{init}} - T^{\text{ref}}$ and $c_{p,2}^{\text{init}} = T_p^{\text{init}} - T^{\text{ref}}$ are the initial temperatures in the bulk and stationary phases. For an initially regenerated column, $c_{b,1}^{\text{init}} = 0$ and $c_{p,1}^{\text{init}} = 0$. Moreover, the following Robin type boundary conditions also known as the Danckwert boundary conditions are considered at the column entrance:

$$-\frac{1}{\text{Pe}_m}\frac{\partial c_{b,m}}{\partial x} + c_{b,m}\bigg|_{x=0} = \begin{cases} c_{b,m}^{\text{inj}}, & \text{if} \quad 0 \le \tau \le \tau^{\text{inj}} \\ 0, & \tau > \tau^{\text{inj}} \end{cases} \tag{14}$$

where $c_{b,1}^{\text{inj}}$ is the inlet concentration, $c_{b,2}^{\text{inj}} = T_b^{\text{inj}} - T^{\text{ref}}$ describes the sample temperature at the inlet and $\tau^{\text{inj}} = ut^{\text{inj}}/L$. At the column outlet ($x = 1$), the following outflow boundary conditions are assumed:

$$\frac{\partial c_{b,m}}{\partial x}\bigg|_{x=1} = 0 \tag{15}$$

boundary conditions for eq. (8), at the center, *i.e.* at $r = 0$ and at the boundary of the porous particle, *i.e.* at $r = 0$ are stated:

$$\frac{\partial c_{p,m}}{\partial r}\bigg|_{r=0} = 0, \quad \frac{\partial c_{p,m}}{\partial r}\bigg|_{r=1} = \text{B}_m\left(c_{b,m} - c_{p,m}\,|_{r=1}\right), \quad \text{for} \quad m = 1,2 \tag{16}$$

where $\text{B}_c = \text{B}_1$ and $\text{B}_T = \text{B}_2$. The formulation of model equations is complete now. The next step is to derive the analytical solution of the model equations.

Procedure for deriving analytical solutions

The considered linearized non-isothermal GRM along with the aforementioned conditions is solved analytically by means of Laplace transformation, the eigenvalue-decomposition technique, and a standard technique for the solutions of ODE. The Laplace transform can be defined:

$$\overline{\zeta}(x,s) = \int_0^\infty \exp(-s\tau)\zeta(x,\tau)\,\text{d}\tau, \quad \tau \ge 0$$

The implementation of Laplace transformation on eq. (8) gives:

$$s\overline{c}_{b,m} + \frac{\partial \overline{c}_{b,m}}{\partial x} = \frac{1}{\text{Pe}_m}\frac{\partial^2 \overline{c}_{b,m}}{\partial x^2} - \xi_m\left(\overline{c}_{b,m} - \overline{c}_{p,m}\,|_{r=1}\right), \quad \text{for} \quad m = 1,2 \tag{17}$$

Using eq. (12) in eqs. (9) and (10) and applying the Laplace transformations, we obtain:

$$\frac{\text{d}^2}{\text{d}r^2}\begin{bmatrix} r\overline{c}_{p,1} \\ r\overline{c}_{p,2} \end{bmatrix} = \begin{pmatrix} \alpha_1 & \alpha_2 \\ \beta_1 & \beta_2 \end{pmatrix}\begin{bmatrix} sr\overline{c}_{p,1} \\ sr\overline{c}_{p,2} \end{bmatrix} \tag{18}$$

where

$$\alpha_1 = \frac{1}{\eta_c}\left[\epsilon_p + (1-\epsilon_p)a^{\text{ref}}\right], \quad \alpha_2 = \frac{1}{\eta_c}\left[\frac{a^{\text{ref}}c^{\text{ref}}(1-\epsilon_p)\Delta H_A}{\text{R}_\text{g}(T^{\text{ref}})^2}\right]$$
$$\beta_1 = \frac{1}{\eta_T}\left[\frac{a^{\text{ref}}(1-\epsilon_p)\Delta H_A}{\rho^L c_P^L}\right], \quad \beta_2 = \frac{1}{\eta_T}\left[\epsilon_p + \frac{(1-\epsilon_p)\rho^s c_P^s}{\rho^L c_P^L} + \frac{a^{\text{ref}}c^{\text{ref}}(1-\epsilon_p)\Delta H_A^2}{\rho^L c_P^L \text{R}_\text{g}(T^{\text{ref}})^2}\right] \tag{19}$$

Equation (18) represents coupled system of differential equations, thus to derive analytical solution, we have to uncouple this system of equation by means of eigenvalue-decomposition technique. The matrix of coefficients on the right side of eq. (18) is diagonalizable and the two distinct eigen values are:

$$\lambda_{1,2} = \frac{1}{2}(\alpha_1 + \beta_2) \pm \frac{1}{2}\sqrt{(\alpha_1 - \beta_2)^2 + 4\alpha_2\beta_1} \tag{20}$$

The corresponding eigenvectors are expressed as:

$$x_1 = \begin{bmatrix} \lambda_1 - \beta_2 \\ \beta_1 \end{bmatrix}, \; x_2 = \begin{bmatrix} \lambda_2 - \beta_2 \\ \beta_1 \end{bmatrix} \tag{21}$$

On the basis of these eigenvalues, the matirx, A of linear transformation can be defined:

$$A = \begin{pmatrix} \lambda_1 - \beta_2 & \lambda_2 - \beta_2 \\ \beta_1 & \beta_1 \end{pmatrix} \tag{22}$$

The effective use of previous matrix helps us to formulate a linear-transformation of the form:

$$\begin{bmatrix} \overline{c}_{p,1} \\ \overline{c}_{p,2} \end{bmatrix} = \begin{pmatrix} \lambda_1 - \beta_2 & \lambda_2 - \beta_2 \\ \beta_1 & \beta_1 \end{pmatrix} \begin{bmatrix} \overline{b}_{p,1} \\ \overline{b}_{p,2} \end{bmatrix} \tag{23}$$

The application of aforementioned linear-transformation on eq. (18) gives:

$$\frac{\mathrm{d}^2}{\mathrm{d}r^2} \begin{bmatrix} r\overline{b}_{p,1} \\ r\overline{b}_{p,2} \end{bmatrix} = \begin{pmatrix} \lambda_1 & 0 \\ 0 & \lambda_2 \end{pmatrix} \begin{bmatrix} sr\overline{b}_{p,1} \\ sr\overline{b}_{p,2} \end{bmatrix} \tag{24}$$

Equation (24) depicts a system of two uncoupled ODE which can be solved explicitly. Their solutions are given:

$$\overline{b}_{p,1}(x,s,r) = \frac{1}{r}[C_1 \mathrm{e}^{\sqrt{s\lambda_1}r} + C_2 \mathrm{e}^{-\sqrt{s\lambda_1}r}], \; \overline{b}_{p,2}(x,s,r) = \frac{1}{r}[D_1 \mathrm{e}^{\sqrt{s\lambda_2}r} + D_2 \mathrm{e}^{-\sqrt{s\lambda_2}r}]. \tag{25}$$

where C_1, C_2, D_1, and D_2 are integrations constants which can be calculated by utilizing the considered boundary conditions at the two ends of the column. Implementing the linear transformation in eq. (23) on the boundary conditions given in eq. (16) at $r = 0$, and then utilizing the resulting boundary conditions in eq. (25), we get $C_1 = -C_2$ and $D_1 = -D_2$. Thus, eq. (25) reduces to:

$$\overline{b}_{p,1}(x,s,r) = \frac{2C_1}{r}\sinh\left(\sqrt{s\lambda_1}r\right), \quad \overline{b}_{p,2}(x,s,r) = \frac{2D_1}{r}\sinh\left(\sqrt{s\lambda_2}r\right) \tag{26}$$

Substituting the values of $\overline{b}_{p,1}$ and $\overline{b}_{p,2}$ in the transformation eq. (23), we obtain:

$$\begin{aligned} \overline{c}_{p,1}(x,s,r) &= (\lambda_1 - \beta_2)\left[\frac{2C_1}{r}\sinh\left(\sqrt{s\lambda_1}r\right)\right] + (\lambda_2 - \beta_2)\left[\frac{2D_1}{r}\sinh\left(\sqrt{s\lambda_2}r\right)\right] \\ \overline{c}_{p,2}(x,s,r) &= \beta_1\left[\frac{2C_1}{r}\sinh\left(\sqrt{s\lambda_1}r\right)\right] + \beta_1\left[\frac{2D_1}{r}\sinh\left(\sqrt{s\lambda_2}r\right)\right] \end{aligned} \tag{27}$$

By utilizing the boundary conditions at $r = 1$ from eq. (16) in eq. (27), we get two coupled equations containing C_1 and D_1. After solving these equations, we obtain:

$$C_1 = \frac{1}{2\sinh\left(\sqrt{s\lambda_1}\right)}\left[\frac{\phi_1(s)}{\upsilon(s)}\overline{c}_{b,1} - \frac{\phi_2(s)}{\upsilon(s)}\overline{c}_{b,2}\right],\ D_1 = \frac{-1}{2\sinh\left(\sqrt{s\lambda_2}\right)}\left[\frac{\phi_3(s)}{\upsilon(s)}\overline{c}_{b,1} - \frac{\phi_4(s)}{\upsilon(s)}\overline{c}_{b,2}\right] \tag{28}$$

where

$$\begin{aligned}
&\phi_1(s) = \mathrm{B}_c[\mathrm{B}_T - 1 + \sqrt{s\lambda_2}\coth\left(\sqrt{s\lambda_2}\right)],\ \phi_2(s) = \frac{(\lambda_2-\beta_2)\mathrm{B}_T}{\beta_1}\left[\mathrm{B}_c - 1 + \sqrt{s\lambda_2}\coth\left(\sqrt{s\lambda_2}\right)\right]\\
&\phi_3(s) = \mathrm{B}_c\left[\mathrm{B}_T - 1 + \sqrt{s\lambda_1}\coth\left(\sqrt{s\lambda_1}\right)\right],\ \phi_4(s) = \frac{(\lambda_1-\beta_2)\mathrm{B}_T}{\beta_1}\left[\mathrm{B}_c - 1 + \sqrt{s\lambda_1}\coth\left(\sqrt{s\lambda_1}\right)\right]\\
&\upsilon(s) = (\lambda_2-\beta_2)\left[\mathrm{B}_c - 1 + \sqrt{s\lambda_2}\coth\left(\sqrt{s\lambda_2}\right)\right]\left[\mathrm{B}_T - 1 + \sqrt{s\lambda_1}\coth\left(\sqrt{s\lambda_1}\right)\right] -\\
&\quad -(\lambda_1-\beta_2)\left[\mathrm{B}_c - 1 + \sqrt{s\lambda_1}\coth\left(\sqrt{s\lambda_1}\right)\right]\left[\mathrm{B}_T - 1 + \sqrt{s\lambda_2}\coth\left(\sqrt{s\lambda_2}\right)\right]
\end{aligned} \tag{29}$$

Using these values in eq. (27), we get:

$$\overline{c}_{p,1}\Big|_{r=1} = \left[\frac{(\lambda_1-\beta_2)\phi_1(s)}{\upsilon(s)} - \frac{(\lambda_2-\beta_2)\phi_3(s)}{\upsilon(s)}\right]\overline{c}_{b,1} - \left[\frac{(\lambda_1-\beta_2)\phi_2(s)}{\upsilon(s)} - \frac{(\lambda_2-\beta_2)\phi_4(s)}{\upsilon(s)}\right]\overline{c}_{b,2} \tag{30}$$

$$\overline{c}_{p,2}\Big|_{r=1} = \beta_1\left[\frac{\phi_1(s)}{\upsilon(s)} - \frac{\phi_3(s)}{\upsilon(s)}\right]\overline{c}_{b,1} + \beta_1\left[\frac{\phi_4(s)}{\upsilon(s)} - \frac{\phi_2(s)}{\upsilon(s)}\right]\overline{c}_{b,2} \tag{31}$$

Substituting the values of $\overline{c}_{p,1}$ and $\overline{c}_{p,2}$ from eqs. (30) and (31) in eq. (17), we have the system of equations:

$$\frac{\mathrm{d}^2}{\mathrm{d}x^2}\begin{pmatrix}\overline{c}_{b,1}\\ \overline{c}_{b,2}\end{pmatrix} - \begin{bmatrix}\mathrm{Pe}_e & \\ & \mathrm{Pe}_T\end{bmatrix}\frac{\mathrm{d}}{\mathrm{d}x}\begin{pmatrix}\overline{c}_{b,1}\\ \overline{c}_{b,2}\end{pmatrix} + \begin{bmatrix}-\gamma_1(s) - s\mathrm{Pe}_e & \gamma_2(s)\\ \gamma_3(s) & -\gamma_4(s) - s\mathrm{Pe}_T\end{bmatrix}\begin{pmatrix}\overline{c}_{b,1}\\ \overline{c}_{b,2}\end{pmatrix} = \begin{pmatrix}0\\0\end{pmatrix} \tag{32}$$

where

$$\begin{aligned}
\gamma_1(s) &= \mathrm{Pe}_e\xi_c\left[1 - \frac{(\lambda_1-\beta_2)\phi_1(s)}{\upsilon(s)} + \frac{(\lambda_2-\beta_2)\phi_3(s)}{\upsilon(s)}\right]\\
\gamma_2(s) &= -\mathrm{Pe}_e\xi_c\left[\frac{(\lambda_1-\beta_2)\phi_2(s)}{\upsilon(s)} - \frac{(\lambda_2-\beta_2)\phi_4(s)}{\upsilon(s)}\right]\\
\gamma_3(s) &= \mathrm{Pe}_T\xi_T\beta_1\left[\frac{\phi_1(s)}{\upsilon(s)} - \frac{\phi_3(s)}{\upsilon(s)}\right],\ \gamma_4(s) = \mathrm{Pe}_T\xi_T\left\{1 - \beta_1\left[\frac{\phi_4(s)}{\upsilon(s)} - \frac{\phi_2(s)}{\upsilon(s)}\right]\right\}
\end{aligned} \tag{33}$$

Equation (32) is a coupled sytem of equations. Again adopting the same decoupling procedure, we can uncouple this system by using the transformation:

$$\begin{pmatrix}\overline{c}_{b,1}\\ \overline{c}_{b,2}\end{pmatrix} = \begin{pmatrix}\lambda_3 - \beta_2'(s) & \lambda_4 - \beta_2'(s)\\ \beta_1'(s) & \beta_1'(s)\end{pmatrix}\begin{pmatrix}\overline{b}_{b,1}\\ \overline{b}_{b,2}\end{pmatrix} \text{ where} \tag{34}$$

$$\alpha_1'(s) = -\gamma_1(s) - s\mathrm{Pe}_e,\ \alpha_2'(s) = \gamma_2(s),\ \beta_1'(s) = \gamma_3(s),\ \beta_2'(s) = -\gamma_4(s) - s\mathrm{Pe}_T$$

$$\lambda_{3,4} = \frac{1}{2}\left[\alpha_1'(s) + \beta_2'(s)\right] \pm \frac{1}{2}\sqrt{\left[\alpha_1'(s) - \beta_2'(s)\right]^2 + 4\alpha_2'(s)\beta_1'(s)} \tag{35}$$

Thus, we achieve an uncoupled system of the form:

$$\frac{\mathrm{d}^2}{\mathrm{d}x^2}\begin{pmatrix}\overline{b}_{b,1}\\ \overline{b}_{b,2}\end{pmatrix} - \begin{bmatrix}\mathrm{Pe}_e & \\ & \mathrm{Pe}_T\end{bmatrix}\frac{\mathrm{d}}{\mathrm{d}x}\begin{pmatrix}\overline{b}_{b,1}\\ \overline{b}_{b,2}\end{pmatrix} + \begin{bmatrix}\lambda_3 & 0\\ 0 & \lambda_4\end{bmatrix}\begin{pmatrix}\overline{b}_{b,1}\\ \overline{b}_{b,2}\end{pmatrix} = \begin{pmatrix}0\\0\end{pmatrix} \tag{36}$$

The solutions of eq. (36) are given:

$$\overline{b}_{b,1}(x,s) = C_1' e^{m_1 x} + C_2' e^{m_2 x},\ \overline{b}_{b,2}(x,s) = D_1' e^{n_1 x} + D_2' e^{n_2 x} \tag{37}$$

where

$$m_{1,2} = \frac{1}{2}\mathrm{Pe}_e \pm \frac{1}{2}\sqrt{\mathrm{Pe}_e^2 - 4\lambda_3},\ n_{1,2} = \frac{1}{2}\mathrm{Pe}_T \pm \frac{1}{2}\sqrt{\mathrm{Pe}_T^2 - 4\lambda_4} \tag{38}$$

where C_1', C_2', D_1' and D_2' are integrations constants that can be calculated by utilizing the considered boundary conditions at both ends of the column. The Laplace transformation of boundary conditions in eqs. (14) and (15) provides:

$$-\frac{1}{\mathrm{Pe}_m}\frac{\partial \overline{c}_{b,m}}{\partial x} + \overline{c}_{b,m}\bigg|_{x=0} = \frac{c_{b,m}^{\mathrm{inj}}}{s}\left(1 - e^{-s\tau^{\mathrm{inj}}}\right),\ \frac{\partial c_{b,m}}{\partial x}\bigg|_{x=1} = 0 \ \text{ for } \ m = 1,2 \tag{39}$$

Utilizing these boundary conditions together with the transformation mentioned in eq. (34), we obtain the following Laplace domain solutions for concentration and temperature:

$$\overline{c}_{b,1} = \frac{\left(1 - e^{-s\tau^{\mathrm{inj}}}\right)c_{b,1}^{\mathrm{inj}}}{(\lambda_3 - \lambda_4)s}\left\{\frac{(\lambda_3 - \beta_2')}{\mu_1}\left[m_1 e^{m_2 x} - m_2 e^{m_1(x-1)+m_2}\right] - \frac{(\lambda_4 - \beta_2')}{\mu_2}\left[n_1 e^{n_2 x} - n_2 e^{n_1(x-1)+n_2}\right]\right\} +$$
$$+\frac{\left(1 - e^{-s\tau^{\mathrm{inj}}}\right)c_{b,2}^{\mathrm{inj}}(\lambda_3 - \beta_2')(\lambda_4 - \beta_2')}{\beta_1'(\lambda_3 - \lambda_4)s}\left\{\frac{-1}{\mu_1}\left[m_1 e^{m_2 x} - m_2 e^{m_1(x-1)+m_2}\right] + \frac{1}{\mu_2}\left[n_1 e^{n_2 x} - n_2 e^{n_1(x-1)+n_2}\right]\right\} \tag{40}$$

$$\overline{c}_{b,2} = \frac{\left(1 - e^{-s\tau^{\mathrm{inj}}}\right)\beta_1' c_{b,1}^{\mathrm{inj}}}{(\lambda_3 - \lambda_4)s}\left\{\frac{1}{\mu_1}\left[m_1 e^{m_2 x} - m_2 e^{m_1(x-1)+m_2}\right] - \frac{1}{\mu_2}\left[n_1 e^{n_2 x} - n_2 e^{n_1(x-1)+n_2}\right]\right\} +$$
$$+\frac{\left(1 - e^{-s\tau^{\mathrm{inj}}}\right)c_{b,2}^{\mathrm{inj}}}{(\lambda_3 - \lambda_4)s}\left\{\frac{(\beta_2' - \lambda_4)}{\mu_1}\left[-m_2 e^{m_1(x-1)+m_2} + m_1 e^{m_2 x}\right] + \frac{(\lambda_3 - \beta_2')}{\mu_2}\left[n_1 e^{n_2 x} - n_2 e^{n_1(x-1)+n_2}\right]\right\} \tag{41}$$

where

$$\mu_1 = m_1\left[1 - \frac{m_2}{m_1}e^{m_2 - m_1} - \frac{m_2}{\mathrm{Pe}_e} + \frac{m_2}{\mathrm{Pe}_e}e^{m_2 - m_1}\right],\ \mu_2 = n_1\left[1 - \frac{n_2}{n_1}e^{n_2 - n_1} - \frac{n_2}{\mathrm{Pe}_T} + \frac{n_2}{\mathrm{Pe}_T}e^{n_2 - n_1}\right] \tag{42}$$

It is very difficult to perform Laplace inversion of the previous equations analytically. For that reason, an accurate and efficient numerical Laplace inversions is suggested to obtain solutions in the time domain, see [25, 28].

Numerical test problems

This section presents some numerical test cases for analyzing profiles of concentration $c_{b,1}$ and temperature $c_{b,2}$ at the column outlet obtained from the semi-analytical solutions, c.f. eqs. (40) and (41), of non-isothermal linearized GRM based on the isotherm given by the eq. (12). To explore the ranges of applicability and to obtain confidence on the correctness of our semi-analytical solutions, a high resolution finite volume scheme (HR-FVS) is also applied is to approximate the non-linear model, c.f. eqs. (8)-(10), [24]. The standard values of the parameters used in the test cases are given in tab. 1. These values fall in the typical ranges of the values which are utilized in HPLC applications [21].

Table 1. Reference parameters used in case studies

Parameters	Values
Column length	$L = 1$ cm
External porosity	$\epsilon_b = 0.4$
Internal porosity	$\epsilon_p = 0.333$
Henry's constant	$a^{\text{ref}} = 1.2$
Particle radius	$R_p = 0.004$ cm
Gas constant	$R_g = 0.008314$ kJ/molK
Density time heat capacity in mobile phase	$\rho^L c_P^L = 4.0$ kJ/ℓK
Density time heat capacity in stationary phase	$\rho^S c_P^S = 4.0$ kJ/ℓK
heat transfer coefficient	$h_{\text{eff}} = 0.1$ J/mincm^2/K
Interstitial velocity	$u = 0.2$ cm per minute
Initial concentration	$c_{b,m}^{\text{init}} = 0$ mol/ℓ
Injected bulk concentration	$c_{b,m}^{\text{inj}} = 1.0$ mol/ℓ
Injected temperature	$T^{\text{inj}} = 300$ K
Reference temperature	$T^{\text{ref}} = 300$ K
Dimensionless injection time	$\tau^{\text{inj}} = 0.3$ minutes
Peclet number for concentration	$\text{Pe}_c = 600$
Peclet number for temperature	$\text{Pe}_T = 600$
Biot number for concentration	$B_c = 40$
Biot number for temperature	$B_T = 68.6$
Dimensioless constant	$\eta_c = 3.1$
Dimensioless constant	$\eta_T = 18.2$

Comparison of isothermal ($\Delta H_A = 0$) and non-isothermal case ($\Delta H_A \neq 0$)

Figure 1 demonstrates a comparison between the isothermal ($\Delta H_A = 0$) and non-isothermal ($\Delta H_A \neq 0$) behavior of the process. In this case, the injected temperature T^{inj} and initial temperature T^{init} were assumed to be equal to the reference temperature T^{ref} *i.e.* $T^{\text{init}} = T^{\text{inj}} = T^{\text{ref}} = 300$. It is clear from fig. 1(a) that in the isothermal case ($\Delta H_A = 0$) the temperature $c_{b,2}$ has a steady profile. The non-isothermal operating conditions shown in fig. 1(b) reflects that a non-zero value of the adsorption enthalpy ($\Delta H_A = -10$ kJ/mol) has generated significant fluctuations in the temperature profile. However, the considered adsorption enthalpy has no influence on the concentration peak $c_{b,1}$ due to the considered linearization. Further, the adsorption front rises the temperature profile (to about >2.5 K), while the subsequent desorption front reduces the temperature. After the elution, the temperature returns back to the reference value. Due to the selected same values of density times specific heat for solid and liquid phases, the pair of temperature and concentration profiles are propagating at comparable speeds and therefore, have similar mean retention times.

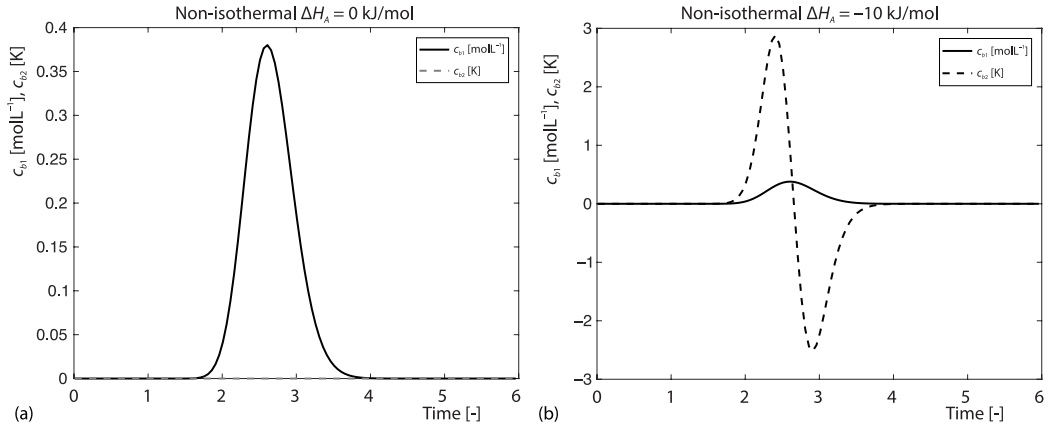

Figure 1. Comparison of isothermal $\Delta H_A = 0$ and non-isothermal $\Delta H_A \neq 0$ cases for $T^{inj} = T^{init} = 300$ K, $\rho^S c_P^S = 4$ kJ/ℓK; other reference parameters are given in tab. 1

Effect of Peclet numbers Pe_c and Pe_T

The specific influences of the dimensionless Peclet numbers, Pe_c (exhibiting axial-dispersion) and Pe_T (exhibiting thermal heat-conductivity along the column) on the temperature and concentration profiles are interpreted in fig. 2, while keeping $T^{inj} = T^{ref}$. It can be seen that a change in the value of Peclet number has a significant impact on the concentration and temperature peaks. The concentration and temperature profiles are widened for small Peclet numbers $Pe_c = Pe_T = 10$ with large variances, while the profiles are more peaked and narrow for larger value of Peclet number $Pe_c = Pe_T = 600$. In the previous calculation, we have chosen $\rho^S c_P^S / \rho^L c_P^L = 1$. It is clearly visible from these plots that Peclet numbers do not influence the holding times of the concentration and temperature profiles.

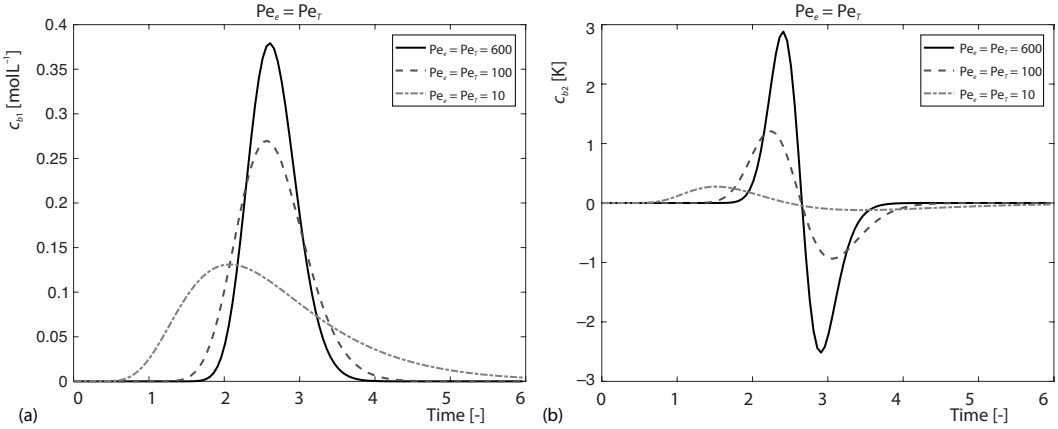

Figure 2. Effect of Peclet number on concentration and temperature profile; $\Delta H_A = -10$ and $\rho^S c_P^S / \rho^L c_P^L = 1$

Effect of enthalpy of adsorption (ΔH_A)

Figure 3 display the effects of different values of adsorption enthalpy on the temperature and concentration profiles. It can be easily seen that analytical results of the consider

linearized model, eq. (12), and numerical results of the HR-FVS for the non-linear isotherm, eq. (5), deviate from each other when the absolute value of adsorption enthalpy is increased from 2-20 kJ/mol. Such bigger values of ΔH_A are the main reasons for profound variations in the temperature profile. For an enthalpy of adsorption $\Delta H_A = -20$ kJ/mol the predicted temperature

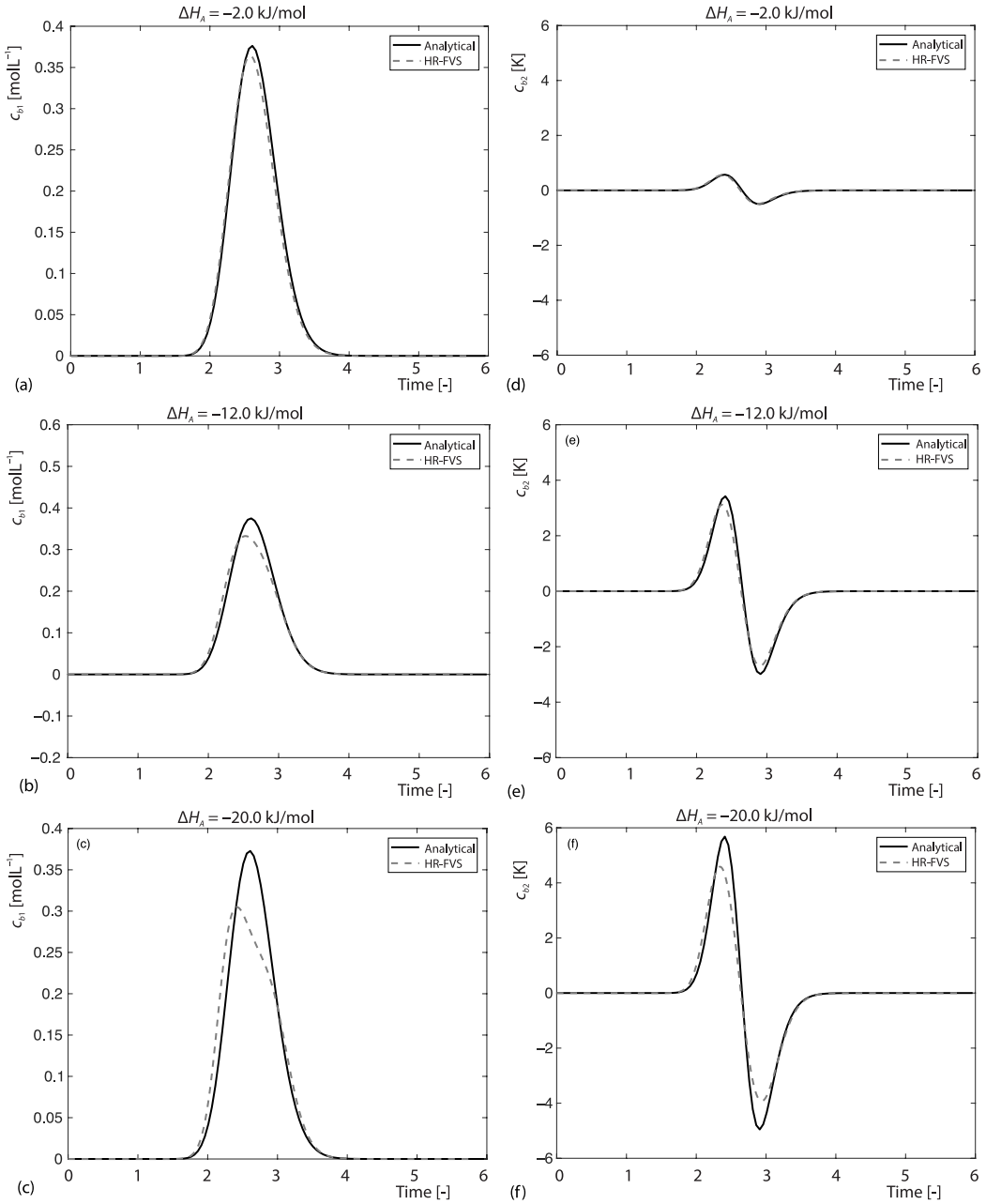

Figure 3. Concentration and temperature peaks at various values of adsorption enthalpy ΔH_A, a comparison of numerical and analytical solutions; $T^{inj} = T^{init} = T^{ref} = 300$ K, $\rho^S c_P^S = 4$ kJ/ℓK, $\rho^L c_P^L = 4$ kJ/ℓK

deviations exceed 5K, fig. 3(f). In the current scenario, our analytical solutions are over-predicting the temperature fluctuations from isothermal level as compared to the more physical numerical solutions and also generate sharper peaks. Thus, these results justify our assumption for linearizing the isotherm for moderate enthalpy of adsorption.

Effect of varying injected temperature $T^{ref} \neq T^{inj}$

Figure 4 demonstrates the behavior of temperature and temperature profiles on varying the temperature of injected sample. In fig. 4(a), it can be observed clearly that due to the considered cold injection $T^{inj} < T^{ref}$, the height of temperature adsorption peak decreases. while, the later occurring temperature desorption peak increases when the temperature of injection is decreased. Contrarily, fig. 4(b) depicts that temperature of adsorption peak lifts up in the positive upward direction due to a *hot injection* $T^{inj} > T^{ref}$. In this situation, the desorption peak gradually declines. In all aforementioned cases, due to small value of adsorption enthalpy and considered linearization, the resulting small temperature variations produce no considerable influence on the profiles of concentration. Once again, we have used $\rho^S c_P^S / \rho^L c_P^L = 1$.

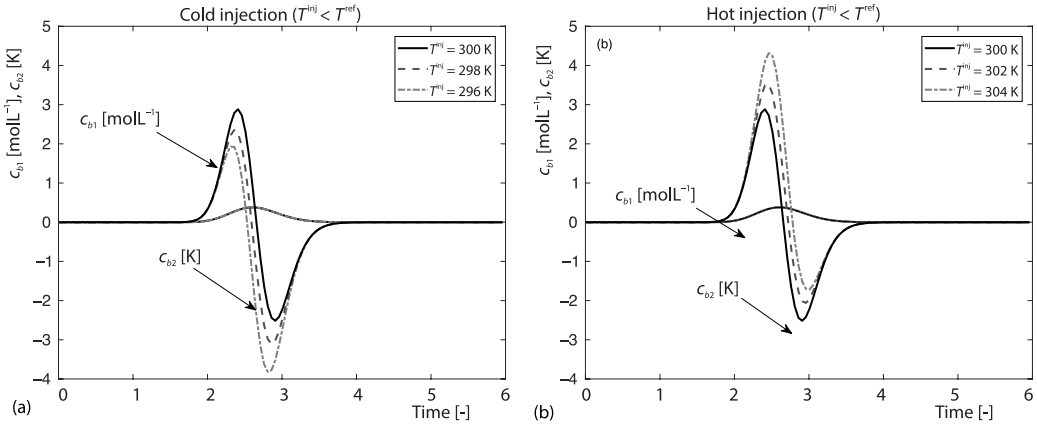

Figure 4. Effect of $T^{ref} = T^{inj}$ and $T^{ref} \neq T^{inj}$ at $\Delta H_A = -10$ and $\rho^S c_P^S / \rho^L c_P^L = 1$ on concentration and temperature profile

Joint effect of Biot number B_c and B_T

Figure 5 describes the joint effects of B_c and B_T. Figures 5(a) and 5(b) show the plots of concentration and temperature, respectively, for three different values of B_T, while keeping $B_c = 40$ as constant. It is evident that with an increase in the value of B_T from 0.686-68.6, broadened peaks of the temperature profiles are converted into narrower peaks. The amplitudes of temperature fluctuations increases for $B_T = 68.6$ and then decreases. Moreover, the variation of B_T has not changed the concentration profile. On the other hand figs. 5(c) and 5(d) displays the plots of concentration and temperature profiles, respectively, for different values of B_c keeping $B_T = 68.6$ as fixed. Now, the variation of B_c has considerable influence on the concentration and temperature peaks. The broadened concentration profiles are shifting to narrower peaks on increasing the value of B_c. In both cases the temperature variations attain an extremum of 1.4 K.

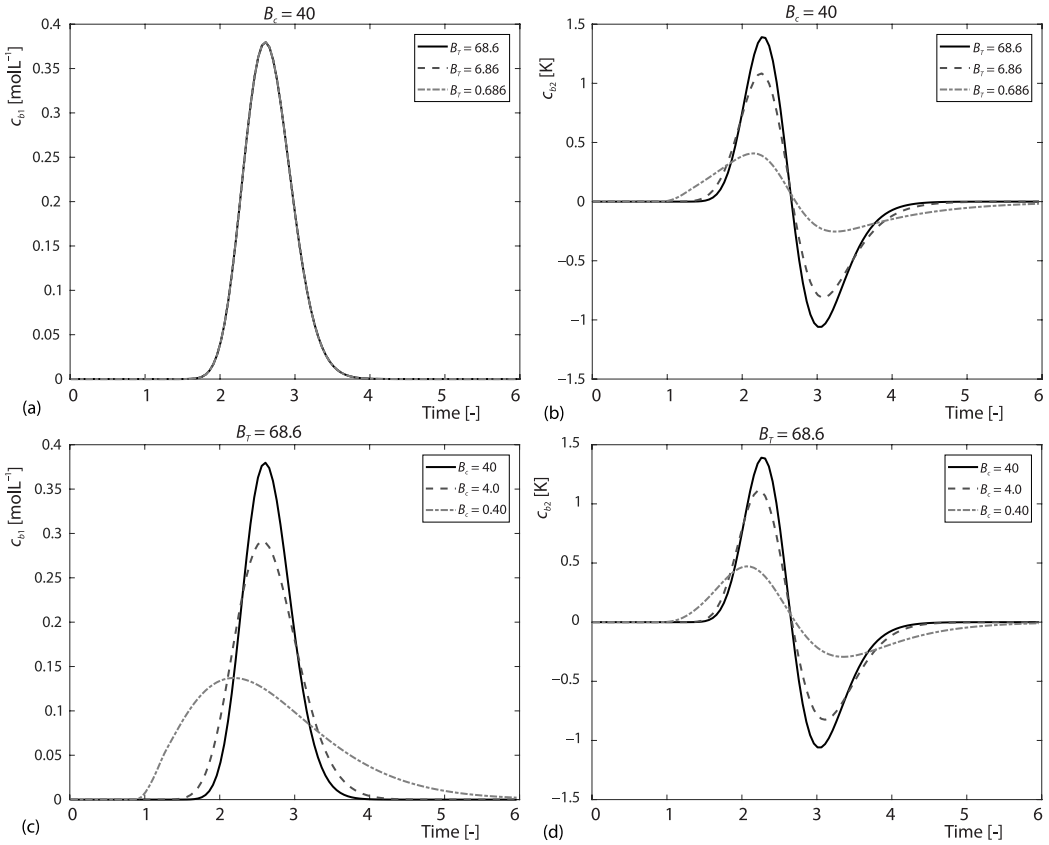

Figure 5. Effect of Biot number on concentration and temperature profile

Influence of dimensionless parameters η_c and η_T

The influence of intraparticle diffusion parameters η_c and η_T on the profiles of concentration and temperature are discussed in fig. 6. Figures 6(a) and 6(b) depict the effect of η_T for a fixed value of η_c, while in figs. 6(c) and 6(d) display the influence of η_c for a fixed η_T. Values of other parameters are listed in tab. 1. The variation in η_T has not changed the concentration profile, while the variation in η_c influences the band broadening of concentration profile. The concentration profile is broadened for small η_c. The amplitudes of temperature fluctuations increases for $\eta_c = 3.1$ and $\eta_T = 18.2$ and then decreases. Further, significant fluctuations are noticed in the temperature profile for different values of η_c.

Effect of the ratio $\rho^S c_P^S / \rho^L c_P^L$

Figure 7 depicts that how a variation in the ratio$\rho^S c_P^S / \rho^L c_P^L$ influences the temperature and concentration profiles, which was taken unity in the previous calculations at $T^{\text{Inj}} = T^{\text{Init}}$. As this ratio varies the mean retention times of the concentration and the temperature profiles, it needs to be discussed separately. Figure 7(a) display the plots of profile for $\rho^L c_P^L / \rho^L c_P^L = 1$ obtained by taking $\rho^L c_P^L = 40$ kJ/ℓK $= \rho^L c_P^L$. For the considered parameters, the fast moving adsorption produces a substantial increase in the temperature, afterward desorption occurs which reduces the temperature. The mean holding times of the temperature and concentration profiles

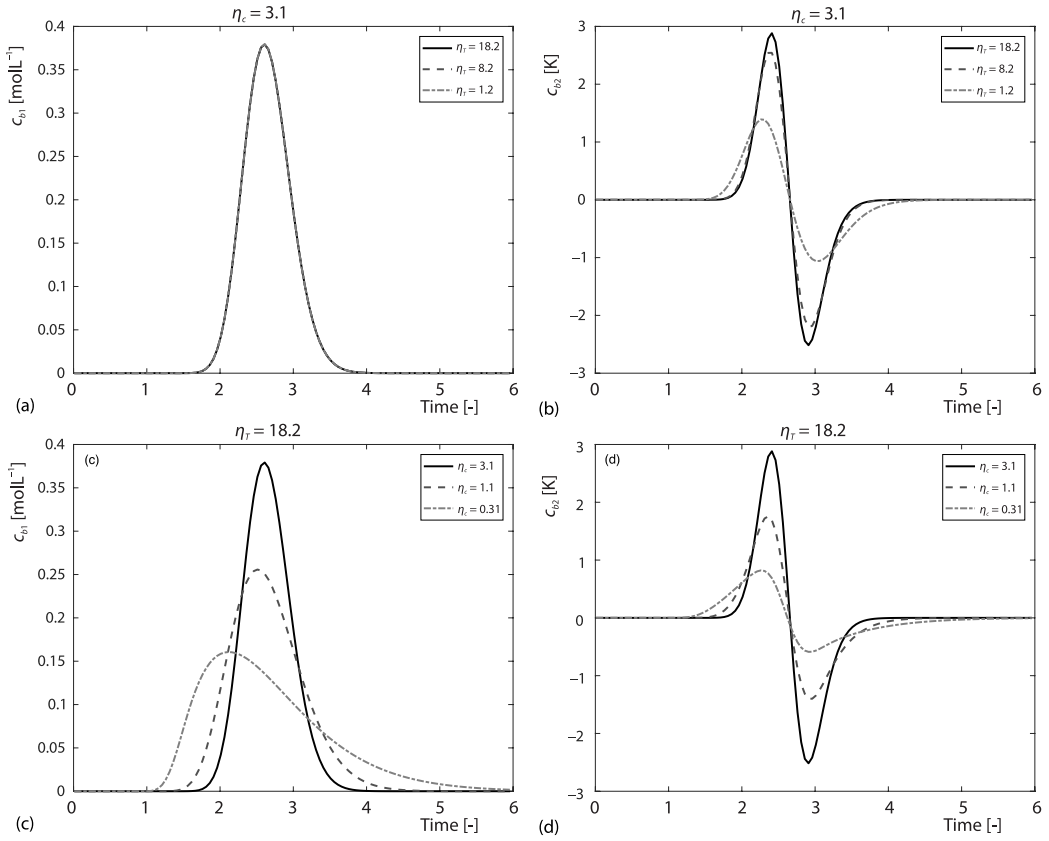

Figure 6. Effect of η on concentration and temperature profile

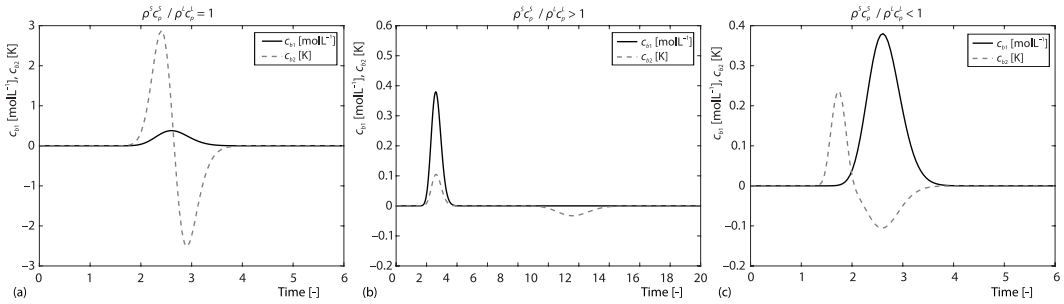

Figure 7. Effect of the ratio $\rho^S c_P^S / \rho^L c_P^L$ on concentration and temperature peaks for $\Delta H_A = -10$ kJ/mol and $T^{inj} = T^{init} = T^{ref}$; (a) $\rho^S c_P^S = \rho^L c_P^L = 40$, (b), $\rho^S c_P^S = 40$, $\rho^L c_P^L = 4$, and (c) $\rho^L c_P^L = 40$, $\rho^S c_P^S = 4$

are very similar and, thus, the two waves travel at similar speeds. Figure 7(b) shows the plots of profile for $\rho^S c_P^S / \rho^S c_P^L = 10$ obtained by taking $\rho^S c_P^S = 40$ kJ/ ℓK and $\rho^L c_P^L = 4$ kJ/ℓK. In the current scenario, the concentration profile has larger velocity compared to the thermal wave. Thus, the positive peak of temperature due to adsorption is moving together with the concentration profile, while the negative peak of temperature caused by desorption elute later from the column. Figure 7(c) shows the plots of profile for $\rho^S c_P^S / \rho^L c_P^L = 0.1$ obtained by taking $\rho^S c_P^S = 4$ kJ/ℓK and $\rho^L c_P^L = 40$ kJ/ℓK. Now, the positive peak of adsorption in the temperature is decoupled and mov-

ing faster than the concentration pulse. On the other hand, the downward peak of desorption in the temperature is coupled with the concentration profile, *i.e.* both are propagating at almost the same speed.

Conclusion

A linearized non-isothermal general rate model was formulated to simulated dynamics of concentration and temperature profiles in a thermally insulated liquid chromatographic column. The solution of the model was derived analytically to analyze the effects of temperature variations on the chromatographic system performance. The Laplace transform, the eigen-decomposition technique, and a conventional technique for the solution of ODE were jointly used to solve the coupled system of differential equations. Various case studies were carried out for analyzing the influence of system parameters on the performance of the column. To access the range of utilization of derived analytical solutions, the numerical results were also obtained by applying a HR-FVS and were compared with the analytical results. It was found that enthalpy of adsorption, ratio of specific heats and temperature of the injected sample are responsible for temperature variation inside the column. The analytical solutions obtained are helpful for further advancements in non-isothermal liquid chromatography.

Nomenclature

a^{ref} – reference Henry's constant, [–]
B_c – Biot number for concentration, [–]
B_T – Biot number for temperature, [–]
c_b – solute concentration in the bulk phase, [molℓ^{-1}]
c_p – solute concentration in the particle pores, [molℓ^{-1}]
$c_{b,i}^{\text{init}}$ – initial concentrations, [molℓ^{-1}]
$c_{b,i}^{\text{inj}}$ – injected bulk concentration, [molℓ^{-1}]
D_b – axial dispersion coefficient, [cm^{2}min^{-1}]
D_{eff} – effective pore diffusivity coefficient, [cm^{2}min^{-1}]
F – phase ratio, [–]
ΔH_A – adsorption enthalpy, [kJmol^{-1}]
h_{eff} – coefficient of heat transfer, [Wcm^{-2}]
L – length of the column, [cm]
k_{eff} – coefficient of effective mass transfer, [min^{-1}]
q_p – solid phase concentration, [molℓ^{-1}]
$\rho^L c_p^L$ – density time heat capacity in liquid phase, [kJℓ^{-1}K^{-1}]
$\rho^S c_p^S$ – density time heat capacity in solid phase, [kJℓ^{-1}K^{-1}]
R – radial-co-ordinate of the spherical particle, [cm]
R_p – radius of particle, [cm]
R_g – general gas constant, [kJmol^{-1}K^{-1}]
T_b – temperature of bulk fluid, [K]
T_p – temperature of particle pore, [K]
T^{inj} – inlet temperature, [K]
T^{init} – initial temperature, [K]
T^{ref} – reference temperature, [K]
t – time co-ordinate, [min]
t^{inj} – injection time, [min]
u – interstatial velocity, [cmmin^{-1}]
z – axial co-ordinate, [–]

Greek symbols

η_c – dimension less constant for concentration,
η_T – dimension less constant for temperature,
$\lambda_{\text{eff},e}$ – heat conductivity coefficient, [KJcm^{-1}]
$\lambda_{\text{eff},z}$ – heat conductivity coefficient, [KJcm^{-1}]
ϵ_b – external porosity, [–]
ϵ_p – internal particle porosity, [–]

References

[1] Guiochon, G., Lin, B., *Modelling for Preparative Chromatography,* Elsevier Academic Press, Amsterdam, The Netherlend, 2003
[2] Guiochon, G., *et al*., *Fundamentals of Preparative and Non-Linear Chromatography*, 2nd ed., Elsevier Academic Press, New York, USA, 2006
[3] Miyabe, K., Guiochon, G., Measurement of the Parameters of the Mass Transfer Kinetics in High Performance Liquid Chromatography, *Journal Sep. Sci*., *26* (2003), 3-4, pp. 155-173
[4] Heinisch, S., Rocca, J. L., Sense and Non-Sense of High-Temperature Liquid Chromatography, *Journal Chromatogr. A.*, *1216* (2009), 4, pp. 642-658

[5] Antia, F, D., Horvath, C., High Performance Liquid Chromatography at Elevated Temperatures: Examination of Conditions for the Rapid Separation of Large Molecules, *Journal Chromatogr. A*., *435* (1988), pp. 1-15
[6] Abbott, S., *et al*., Effects of Radial Thermal Gradients in Elevated Temperature High-Performance Liquid Crhomatography, *Journal Chromatogr*., *218* (1981), Nov., pp. 123-135
[7] Brandt, A., *et al*., Temperature Gradients in Preparative High performance Liquid Chromatography Columns, *Journal Chromatogr. A*., *769* (1997), 1, pp. 109-117
[8] Greibrokk, T., Andersen, T., High Temperature Liquid Chromatography, *Journal Chromatogr. A*., *1000* (2003), 1-2, pp. 743-755
[9] Holm, A., *et al*., Novel Column oven Concept for Cold Spot Large Volume Sample Enrichment in High throughput Temperature Gradient Capillary Liquid Chromatography, *Journal Sep. Sci*., *26* (2003), 12-13, pp. 147-153
[10] Warren, F. V. Jr., Bidlingmeyer, B. A., Influence of Temperature on Column Efficiency in Reversed-Phase Liquid Chromatography, *Anal. Chem*., *60* (1988), 24, pp. 2821-2824
[11] Cerro, R., L., Smith, W., Effects of Heat Release and Non-linear Equilibrium on Transient Adsorption, *Ind. Eng. Chem. Fund*., *8* (1969), 4, pp. 796-802
[12] Glockler, B., *et al*., Efficient Reheating of a Reverseflow Reformer-An experimental study, *Chem.Eng. Sci*., *62* (2007), 18-20, pp. 5638-5643
[13] Kruglov, A., Methanol Synthesis in a Simulated Countercurrent Moving-bed Adsorptive Catalytic Reactor, *Chem. Eng. Sci*., *49* (1994), 24, Part A, pp. 4699-4716
[14] Xiu, G., *et al*., Sorption-Enhanced Reaction Process with Reactive Regeneration, *Chem. Eng. Sci*., *57* (2002), 18, pp. 3893-3908
[15] Yongsunthon, I., Alpay, E., Design of Periodic Adsorptive Reactors for the Optimal Integration of Reaction, Separation and Heat Exchange, *Chem. Eng. Sci*., *54* (1999), 13-14, pp. 2647-2657
[16] Chen, M., H., Horvath, C., Temperature Programming and Gradient Elution in Reversed-Phase Chromatography with Packed Capillary Columns, *Journal Chromatogr. A*., *788* (1997), 1-2, pp. 51-61
[17] Genowefa, H., Jerzy, S., K., The Effect of Temperature on the Efficiency Parameters in Adsorptive Liquid Chromatography, J*HRC*, *4* (1981), pp. 27-32
[18] Sainio, T., Ion-Exchange Resins as Stationary Phase in Reactive Chromatography, Ph. D. thesis, Acta Universitatis Lappeenrantaensis 218, Lappeenranta, University of Technology, Finland
[19] Sainio, T., *et al*., Thermal Effects in Reactive Liquid Chromatography, *Chem. Eng. Sci*., *62* (2007), 18-20, pp. 5674-5681
[20] Sainio, T., *et al*., Adiabatic Operation of Chromatographic Fixed-Bed Reactors, *Chem. Eng. J*., *168* (2011), 2, pp. 861-871
[21] Vu, T. D., Seidel-Morgenstern, A., Quantifying Temperature and Flow Rate Effects on the Performance of a Fixed-Bed Chromatographic Reactor, *Journal Chromatogr. A*., *1218* (2011), 44, pp. 8097-8109
[22] Javeed, S., *et al*., Parametric Study of Thermal Effects in Reactive Liquid Chromatography, *Chem. Eng. J*., *191* (2012), May, pp. 426-440
[23] Qamar, S., *et al*., Theoretical Investigation of Thermal Effects in Non-Isothermal Non-Equilibrium Reactive Liquid Chromatography, *Chem. Eng. Res. Design*., *115* (2016), Sept., pp. 145-159
[24] Qamar, S., *et al*., Theoretical Analysis of the Influence of Forced and Inherent Temperature Fluctuations in an Adiabatic Chromatographic Column, *Chem. Eng. Sci*., *161* (2017), Apr., pp. 249-264
[25] Qamar, S., *et al*., Theoretical Investigation of Thermal Effects in an Adiabatic Chromatographic Column Using a Lumped Kinetic Model Incorporating Heat Transfer Resistances, *Ind.& Eng. Chem. Res*., *57* (2018), 6, pp. 2287-2297
[26] Hayat, A., *et al*., Theoretical Analysis of Forced Segmented Temperature Gradients in Liquid Chromatography, *Processes*, *7* (2019), 11, pp. 846-864
[27] Zafar, S., *et al*., Analysis of Temperature Variation in Fixed-Bed Columns Using Non-Isothermal and Non-Equilibrium Transport Model, *Thermal Science*, On-line first, https://doi.org/10.2298/TSCI200227192Z
[28] Durbin, F., Numerical Inversion of Laplace Transforms: An Efficient Improvement to Dubner and Abate's Method, *Comput. J*., *17* (1974), 4, pp. 371-376

Paper submitted: July 29, 2020
Paper revised: October 26, 2020
Paper accepted: October 27, 2020